
Article:
Silva-Rodriguez, J, Cortes, J, Rodriguez-Osorio, X et al. (4 more authors) (2016) Iterative Structural and Functional Synergistic Resolution Recovery (iSFS-RR) Applied to PET-MR Images in Epilepsy. IEEE Transactions on Nuclear Science, 63 (5). pp. 2434-2442. ISSN 0018-9499

https://doi.org/10.1109/TNS.2016.2527826

Iterative Structural and Functional Synergistic Resolution Recovery (iSFS-RR) applied to PET-MR images in Epilepsy

J. Silva-Rodríguez, J. Cortés, Xiana Rodríguez-Osorio, J. López-Urdaneta, J. Pardo-Montero, P. Aguiar* and C. Tsoumpas

***Abstract*— Structural Functional Synergistic Resolution Recovery (SFS-RR) is a technique that uses supplementary structural information from MR or CT to improve the spatial resolution of PET or SPECT images. This wavelet-based method may have a potential impact on the clinical decision-making on brain focal disorders such as refractory epilepsy, since it can produce images with better quantitative accuracy and enhanced detectability. In this work, a method for the iterative application of SFS-RR (iSFS-RR) was firstly developed and optimized in terms of convergence and input image sizes, and then used for the diagnosis of 18 patients with refractory epilepsy. To this end, PET/MR images were clinically evaluated through visual inspection, atlas-based asymmetry indices (AIs) and SPM analysis, using uncorrected images and images corrected with SFS-RR and iSFS-RR. Our results showed that the sensitivity can be increased from 78% for uncorrected images, to 84% for SFS-RR and 94% for the proposed iSFS-RR. Thus, the proposed methodology has demonstrated the potential to improve the management of refractory epilepsy patients in the clinical routine.**

***Index Terms*— PET-MR, Epilepsy, Partial Volume Correction, Image processing.**

This work was supported in part by public Fondo de Investigaciones Sanitarias (DTS14/00158), MINECO (2014/CSUN1/000004) and the EU COST Action TD1007 (www.pet-mri.eu). P. Aguiar is awarded a public fellowship from Xunta de Galicia (POS-A/2013/00). J. Pardo-Montero acknowledges the support of Instituto de Salud Carlos III (Miguel Servet grant CP12/03162).

Jesús Silva-Rodríguez, Juan Pardo-Montero and Pablo Aguiar (* corresponding author) are with the Molecular Imaging Group in Instituto de Investigación Sanitarias de Santiago de (IDIS), University of Santiago de Compostela. Travesía da Choupana s/n, 15706 Santiago de Compostela, Galicia, Spain (e-mail: pablo.aguiar@usc.es) (e-mail: jesus.silva@usc.es) (e-mail: juan.pardo.monteroa@sergas.es). Julia Cortés and Jesús López-Urdaneta are with the Nuclear Medicine Department, Hospital Clínico, Complexo Hospitalario Universitario de Santiago de Compostela. Travesía da Choupana s/n, 15706 Santiago de Compostela, Galicia, Spain. (e-mail: julia.cortes.hernandez@sergas.es) (e-mail: jesus.lopez.urdaneta@sergas.es). Xiana Rodríguez-Osorio is with the Neurology Department, Hospital Clínico, Complexo Hospitalario Universitario de Santiago de Compostela. Travesía da Choupana s/n, 15706 Santiago de Compostela, Galicia, Spain. (e-mail: xiana.rodriguez.osorio@sergas.es). Dr Charalampos Tsoumpas is with the Division of Biomedical Imaging of the University of Leeds, Worsley Building, LS2 9JT, Leeds, United Kingdom. (e-mail: c.tsoumpas@leeds.ac.uk).

I. INTRODUCTION

POSITRON Emission Tomography (PET) is a non-invasive imaging technique that visualizes the distribution of different radiotracers in the body providing functional and molecular information on tissues. PET is widely used in neurology for *in vivo* examination of brain functionality allowing the quantification of cerebral blood flow, metabolism, receptor binding and many other physiological parameters [1]. It is a valuable tool for the evaluation of Parkinson's disease, Huntington's disease, multiple sclerosis, dementias and epilepsy [2]. In the latter case, PET and subtraction ictal single photon emission computed tomography (SPECT) co-registered to magnetic resonance imaging (MRI), known also as SISCOM, are routinely used as complements for MRI in the localization of the epileptogenic focus before surgery [3] [4]. For this particular application, PET has gained a leading role since it has demonstrated to be simpler than SISCOM and more sensitive than MRI in certain situations [5] [6]. Furthermore, the usability and sensitivity of PET have been increased in the later years by two main facts. First, the availability of co-registered PET/MR images has improved the interpretation of images of both modalities and enabled a more straightforward use of PET information on MRI-guided surgery [7]. Second, the inclusion of PET quantification techniques, such as Atlas-based Asymmetry Indices (AI) and Statistical Parametric Mapping (SPM) on the clinic has improved the localization of the epileptogenic focus [8] [9]. Despite of these advancements, the sensitivity of PET is still relatively low in epilepsy [6] [5] [10] [9], especially when dealing with small focal hypometabolisms, due to the limited resolution of PET images. This is extremely important since the size of the hypometabolism is inversely correlated with the surgery outcome [11]. In this context, techniques that can provide an improvement on PET resolution have a great potential to improve the localization of these small hypometabolisms and consequently the surgery outcome.

In this context, several approaches have been suggested for the use of supplementary MRI-based structural information for the resolution recovery (RR) of PET images [12] [13]. These techniques have some advantages compared to conventional RR approaches modeling the point-spread function (PSF) into the reconstruction, especially due to better noise handling [14] [15]. Furthermore, many reconstruction algorithms exploiting

anatomical information during reconstruction to reduce the noise while keeping the high resolution have been proposed in literature [16] [17]. Recently, the use of an anatomical brain atlas was introduced as a source of structural information for the improvement of PET resolution [12] [18] [19]. The use of high-frequency structural information enhances the resolution of the PET images without significantly altering its functional patterns. One of the most promising techniques using this approach is the Structural Functional Synergistic Resolution Recovery (SFS-RR) [18], which has provided excellent results on simulations, phantoms and in some particular clinical case with both neurology and oncology patients [20] [21] [22] [23]. This methodology may have potential impact in clinical decision-making in epilepsy since it can produce images with enhanced contrast and improved lesion detectability in the visual inspection of PET data. Nevertheless, the method has some shortcomings. First, in SFS-RR an atlas with white and grey matter information obtained from the MRI (usually a T1 image) is filled with quantitative values obtained from the PET image. These values are affected by Partial Volume Effect (PVE), which will limit the accuracy of the correction. Second, wavelet decomposition is a very time consuming process due to the large number of pixels in clinical MR images. The use of larger voxels can remarkably reduce this time demand but it could have an impact on the segmentation accuracy. These limitations should be assessed before the widespread use of this methodology in clinical routine

In this work, we aim at developing, optimizing and evaluating a novel methodology for the iterative application of SFS-RR (iSFS-RR). We evaluate the potential of the developed methodology to provide an improved localization of small focal hypometabolisms and consequently an improvement in the diagnosis of focal disorders such as epilepsy. For this, a group of patients previously diagnosed with refractory epilepsy was re-evaluated using images partial volume corrected with the novel methodology.

II. METHODS

A. SFS-RR

The wavelet transform (WT) provides a framework to decompose images into a number of new images, each one of them with a different degree of resolution [24]. The basic idea of RR using wavelets is to decompose the functional (PET or SPECT) and the structural reference image (MRI, CT or other) into several resolution elements using the wavelet transform (WT) and then replace the high-resolution components of the functional image with the ones of the anatomical image with an appropriate local scaling. This way, details of the high-resolution image are extracted, transformed and integrated into the low-resolution image [25]. The main limitation of wavelet-based RR is that functional and anatomical distributions may differ leading to artifacts or alterations of the functional patterns on the final functional images. To prevent this, the replacement of functional with structural information is performed locally by evaluating the ratio between functional and structural signal in the wavelet domain. However, this may not be sufficient as no single structural image may provide the anatomical support for the functional study at hand. An alternative solution is to use an anatomical

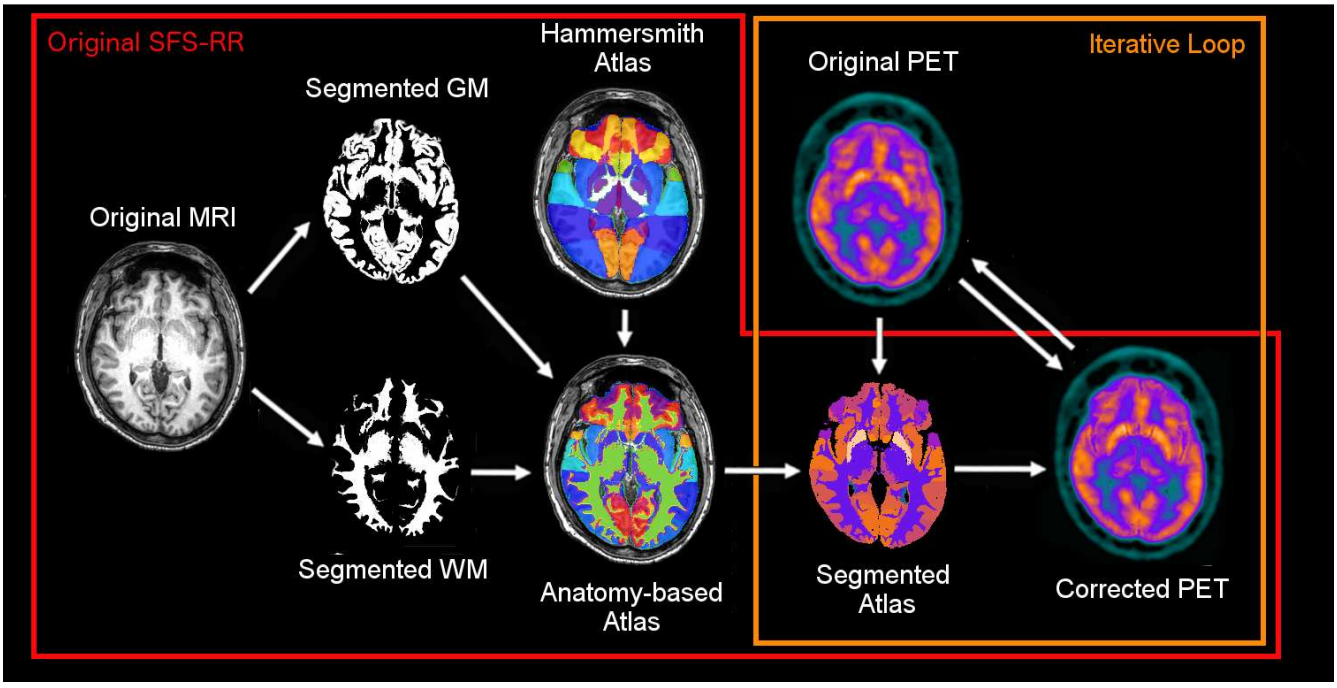

Figure 1: Workflow of SFS-RR and the proposed iSFS-RR.

frequency-based brain atlas as a source of structural information for the RR process [18].

Figure 1 (red box) shows the steps of the SFS-RR correction proposed by Shidahara et al. [18]:

(a) T1-MRI is segmented into white and grey matter and this information combined with the Hammersmith atlas to generate a probabilistic anatomy-based atlas with Regions of Interest (ROIs) for grey and white matter.

(b) Each Region of Interest (ROI) of the generated anatomy-based atlas is filled with the average uptake in the patient's PET scan for each ROI, generating a segmented atlas with anatomical and functional information.

(c) The PET image and the corresponding segmented atlas are decomposed into several resolutions using the dual-tree complex wavelet transform (CWT) [26], which decomposes the image into multiple directional features (six quadrants with directionalities ±15°, ±45° and ±75°).

(d) The high frequencies from the segmented atlas are weighted using three levels of scaling and introduced into the PET data. The high-resolution wavelet coefficients of the corrected image are calculated as:

$$d^{corr} = \beta \cdot \{\gamma \cdot (\alpha \cdot d^{seg}) + (1-\gamma) \cdot d^{PET}\}$$

where $d^{seg}, d^{PET}, d^{corr}$ are the segmented atlas, PET and corrected PET wavelet coefficients, β is a coefficient accounting for the difference in resolutions between the two images, γ is the branching factor that weights anatomical versus functional information and α is a global calibration factor compensating for the different intensity between anatomical and PET wavelet coefficients.

(e) Finally, the PET image is recomposed resolution-recovered.

B. iSFS-RR

The accuracy of SFS-RR when applied to clinical data is limited by PVE, which significantly bias the generation of the PET-based segmented atlas, an essential step of the correction. In this work, we propose an iterative method for the application of the SFS-RR (iSFS-RR), which could potentially solve the PVE problem. Since the output of the SFS-RR is corrected for PVE, it can be used to re-generate the segmented atlas and perform the correction again, obtaining a more accurate result. The wavelet coefficients of the corrected image are for iteration *n* are calculated as:

$$d^{corr(n)} = \beta_n \cdot \{\gamma_n \cdot (\alpha_n \cdot d^{seg(n)}) + (1-\gamma_n) \cdot d^{corr(n-1)}\}$$

where β_n, γ_n and α_n are the updated coefficients. This process can be repeated until the output PET and the segmented atlas are converging to a stable results. Figure 1 (orange box) illustrates the proposed iterative loop. The first iteration of this process is equivalent to the conventional SFS-RR.

C. Patients

In this work we retrospectively re-evaluated images from 18 patients with intractable temporal lobe epilepsy (TLE). These patients have been previously diagnosed and operated by the Refractory Epilepsy Surgery Unit at the University Hospital of Santiago de Compostela in the period 2012-2013. Following the Refractory Epilepsy Surgery Unit protocol, all of them underwent FDG-PET, 3T-MRI, video electro-encephalography and a wide range of neurological and neuropsychological tests. The epilepsy diagnosis and focus localization was obtained evaluating the results coming from the whole group of tests. We also used images from 97 control subjects. These images were obtained from pre-treatment oncologic patients that underwent FDG-PET after signed consent. As the oncology protocol in our center fix a waiting time of 1 hour and the brain imaging protocol fix a waiting time of 45 minutes, the brain bed was acquired previous to the whole-body PET. All of the control subjects were examined for ensuring that there are no signs of a neurologic or psychiatric disease and the obtained images were evaluated by two experienced nuclear medicine physicians and were considered normal. All the images were acquired following the protocols detailed below.

D. Imaging protocols

a) *FDG-PET*: all patients underwent the routine neuroimaging protocol at our institution. The patient lays at rest in a dark and quiet room after intravenous injection of 370 MBq of ^{18}F-FDG. Starting 45 min after injection, the patient was scanned during 30 min for emission data and 15 min for transmission data, required for attenuation correction. The imaging device was a GE Advance NXi PET scanner (General Electrics Healthcare, Little Chalfont, Buckinghamshire, United Kingdom). Following the default protocols of the GE Advance, scatter, randoms, attenuation and normalization corrections were applied before the reconstruction. PSF modeling and motion correction were included. The images were reconstructed using 3D ordered subsets expectation maximization (3D-OSEM), with 4 subsets and 16 iterations. The size of the reconstructed image is 128x128x35, with a voxel size of 2×2×4.25 mm^3. No smoothing was applied during or after the reconstruction.

b) *3T-MRI*: structural imaging was performed with an Achieva 3.0T X-series MR imaging scanner (Philips Healthcare, Best, The Netherlands) using a head coil. The MRI protocol consisted of the acquisition of T1-weighted 3D TFE, FLAIR and T2-weighted sequences. The different sequences were visually evaluated for diagnosis following the protocols of the Refractory Epilepsy Surgery Unit. Additionally, the T1-weighted 3D TFE was used as an input for the PVE correction.

E. Image Analysis

PET and T1-MRI sequences were co-registered and analyzed using statistical parametric mapping (SPM) software package (SPM12, Wellcome Trust Centre for Neuroimaging,

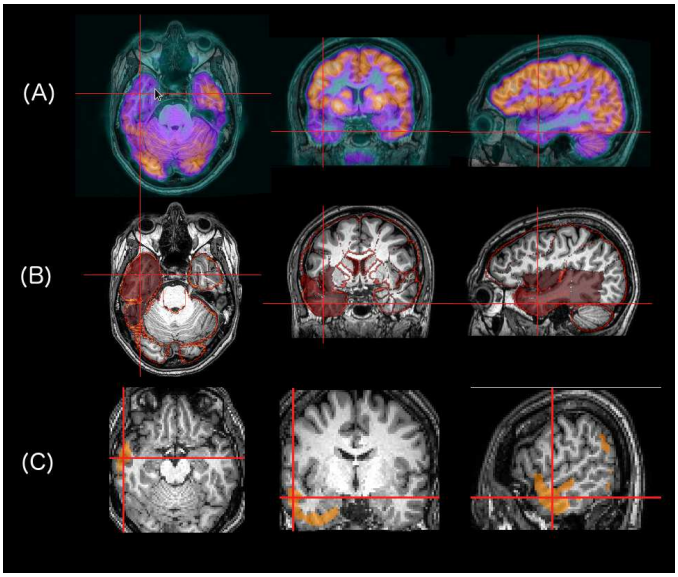

Figure 2: Example of the performed image analysis. PET/MR co-registered images showing a hypometabolism on the right temporal lobe (A), Asymmetrical ROIs from the AI analysis (B) and results of the voxel-by-voxel comparison from SPM (C). In (C) images are shown in the Montreal Neurological Institute space.

University College London, United Kingdom). PET images were evaluated using visual inspection of PET/MR co-registered images, calculations of asymmetry indices (AI) and a voxel-by-voxel statistical comparison. Figure 2 shows an example of the results of the performed analysis.

a) PET/MR co-registering: The co-register of T1-MRI and PET images was performed with the SPM package. The used algorithm is similar to the one presented by Collignon et al. [27]. The original interpolation method described in this paper has been changed in order to give a smoother cost function in order to make the cost function as smooth as possible, to give faster convergence and less chance of local minima. The co-registered PET has the same matrix and pixel size of the MR image.

b) Asymmetry Indices: The asymmetry calculations were based on the ROIs of the Hammersmith atlas [28], specifically designed for TLE. The group of 97 control subjects was used for generating a template of the average uptake of the healthy brain on the Montreal Neurological Institute (MNI). The original T1-MRI images were normalized to the MNI space using SPM. Spatial normalization is done via a segmentation routine [29]. The transformation matrix is inverted and applied to the atlas and the healthy brain template, taking them to the patient space. The PET image (co-registered to the T1-MRI) is proportionally scaled to the healthy brain template to eliminate global differences. Afterwards, differences on the average uptake between the patient PET (VM_p) and the healthy template (VM_c) are calculated for each ROI on the Atlas and contralateral ROIs and are compared to obtain asymmetry indices as:

$$AI(\%) = \left[\frac{(VM_p(L) - VM_c(L))}{VM_c(L)} - \frac{(VM_p(R) - VM_c(R))}{VM_c(R)}\right] X100$$

where L and R stand for left and right sides of the brain. AIs higher than 5% were considered significant based on the intrinsic AI variability obtained from the controls.

c) Voxel-by-voxel analysis: The calculated normalization matrix is applied to the PET image to take it to the MNI space. Afterwards, the patient is compared to the group of 97 healthy patients using a two-sample t-test [30]. All images, including the patient PET image, were smoothed using a 4-mm Gaussian filter. Proportional scaling was used to remove the global differences between subjects. Clusters of 100 pixels with T-scores higher than 3.5 were considered significant.

A positive PET report was emitted when the hypometabolism was observed in the visual inspection (VI) of the PET/MR image and it was reported as positive by the AIs of the SPM of the quantitative analyses *(VI×(AI+SPM))*. Following the aforementioned evaluation protocol, all patients were evaluated by using original PET images and PET images corrected with SFS-RR and with the proposed iSFS-RR method. Figure 1 shows an example of the performed analysis where the 3 tests gave a true localization of the focus.

F. iSFS-RR Convergence Evaluation

The convergence of the was evaluated using subtraction images of corrected PET images of consecutive iterations. To evaluate this global convergence, we measure two parameters, named maximum change (MC) and average change (AC) and defined as:

$$MC\ (\%) = \frac{\max\{abs[it(n) - it(n-1)]\}}{average\ [it(n)]} x100$$

$$AC\ (\%) = \frac{\text{average}\{abs[it(n) - it(n-1)]\}}{average\ [it(n)]} x100$$

were it(n) is the actual iteration and it(n-1) is the previous iteration. We also investigate the impact of different input MRI image sizes on the correction outcome. The latter is especially significant for the high time demand proposed methodology since wavelet decomposition is iteratively performed. To evaluate this, we generated corrected images using inputs of two different sizes: 256×256×175 pixels of 1×1×1 mm^3 and 128×128×87 pixels of 2×2×2 mm^3. The whole process including the segmentation and alignment of the MR and the Hammersmith atlas for the generation of the probabilistic anatomy-based atlas was performed for the two subsets. We evaluated the variations along the iterations of the

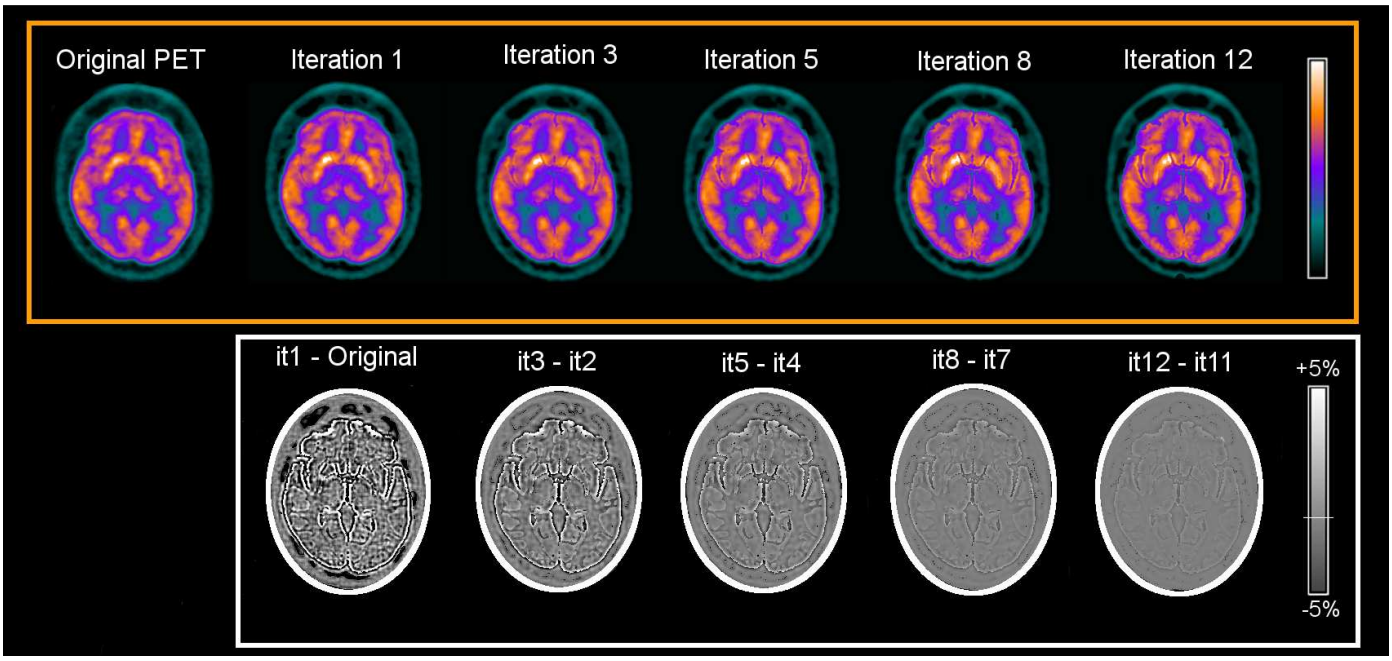

Figure 3: Original PET and corrected images for 1, 3, 5, 8 and 12 iterations (top) and difference images compared with the previous iteration for each of the top images (bottom).

obtained final quantification values (AIs and SPM T-scores) in a sample of 10 patients with previously identified small (5) and extended (5) hypometabolisms.

		AI change (%)		SPM change (%)	
Patient	**H.M. Type**	**128pix**	**256pix**	**128pix**	**256pix**
1	Extended	0,77	2,58	0,00	2,52
2	Extended	1,21	-2,07	-2,55	1,65
3	Extended	6,51	0,61	1,49	2,19
4	Extended	5,78	-0,50	8,19	9,89
5	Extended	5,30	-0,08	4,82	9,84
6	Focal	1,27	-0,09	30,71	17,10
7	Focal	-5,30	-1,54	17,97	12,64
8	Focal	12,58	7,32	19,51	15,17
9	Focal	0,95	-0,58	45,55	52,42
10	Focal	2,43	6,60	16,79	21,46

Table 1: Relative changes of AIs and SPM T-scores for a group of 10 patients for different hypometabolism sizes between original and iSFS-RR corrected PET images.; [(a)]1.5 minutes per iterations (7.5 minutes for 5 iterations); [(b)]5 minutes per iteration (25 minutes for 5 iterations) on Intel Xeon CPU E3-1241 v3 @ 3.50 GHz.

G. Clinical Evaluation

After the convergence evaluation we fixed a number of iterations for applying the iterative method. The optimized protocol was applied to our database of 18 epilepsy patients. A complete patient report was obtained for images corrected with SFS-RR and with the proposed iSFS-RR. The clinical evaluation was performed with images of 256×256×175 pixels of 1×1×1 mm^3 since they were found more convenient for the visual inspection. The results were compared with those of the original PET in order to evaluate the improvements due to the application of SFS-RR and iSFS-RR.

III. RESULTS

A. Optimization of the iSFS-RR

Figure 3 shows the obtained PET images along the iterations for a particular patient. At the bottom of the figure we show the difference images between consecutive iterations for each of the images above. It can be observed in both cases that the method produces images that have visually converged as intended. Figure 4 shows MC and AC values obtained from iteration 1 to 12 for this patient. Convergence was similar for the whole group, ranging from 4-6 iterations for ensuring MC changes below 5% and AC changes below 2%. No correlation was found between the focus size and the needed number of iterations. 6 iterations were finally chosen for the subsequent analysis of iSFS-RR as a reasonable option after balancing accuracy and computing time.

Table 1 shows the relative increase of AI and SPM T-score values after 6 iterations for 128 and 256 input image sizes. The averaged AIs increases were of 3.91% (128 pixels) and 0.11% (256 pixels) for the extended hypometabolisms, and 2.38% (128 pixels) and 2.81% (256 pixels) for the focal hypometabolisms. The averaged T-scores increases were of 2.39% (128 pixels) and 5.21% (256 pixels) for the extended

hypometabolisms and 26.10% (128 pixels) and 23.75% (256 pixels) for the focal hypometabolisms.

Figure 5 shows T-score values along the iterations for patients with extended and focal hypometabolisms (iteration 1 is equivalent to the conventional SFS-RR). It can be observed that T-score values converge after iteration 6 for both focual and extended hypometabolisms. It can be observed that both 128 and 256 pixel image sizes converged similarly based on the analysis of this particular analysis.

B. Clinical Evaluation

Figure 6 shows a visual comparison between original, 128 and 256 pixels corrected images (iSFS-RR, 6 iterations) for a particular patient. We can observe the lesion on the temporal lobe better contrasted on the PVE corrected images. Despite both 128 and 256 pixel corrected images showed similar quantitative results on previous section, it can be observed that 256 pixel images show higher level of detail. The clinical visual inspection was performed on 256 pixel images, where we obtained 14/18 (78%) positives with the uncorrected images, 15/18 (83%) positives with the SFS-RR corrected images, and 17/18 positives (94%) with the proposed iterative methodology. Regarding the quantitative evaluation, the AIs analysis gave a positive localization of the focus for 16/18 (88%) of the patients regardless of the used methodology and the SPM statistical analysis returned 9/18 (50%) positives for uncorrected images, 12/18 (66%) for SFS-RR corrected images and 14/18 (78%) for the proposed methodology. The final PET report gave a positive

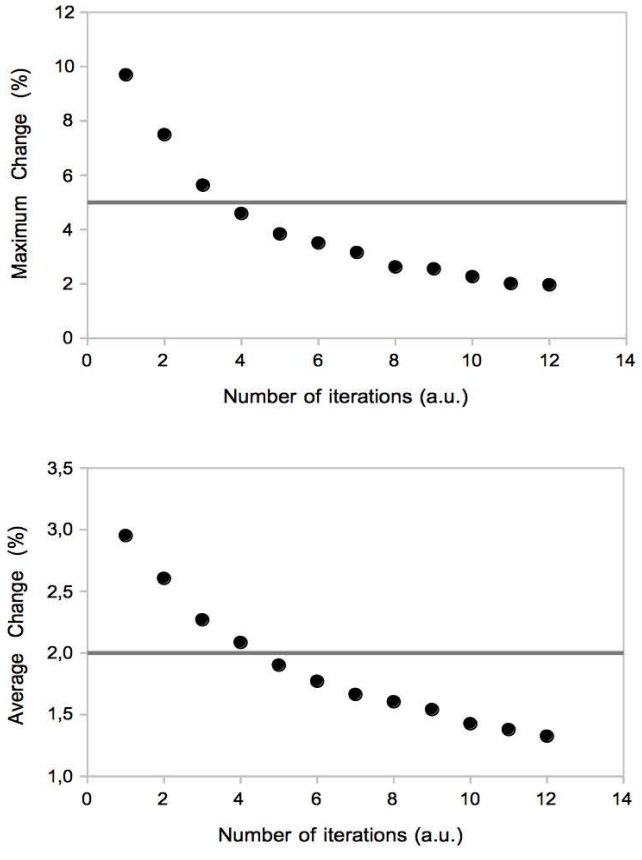

Figure 4: Maximum and average change per voxel for each iteration from 1 to 12 iterations.

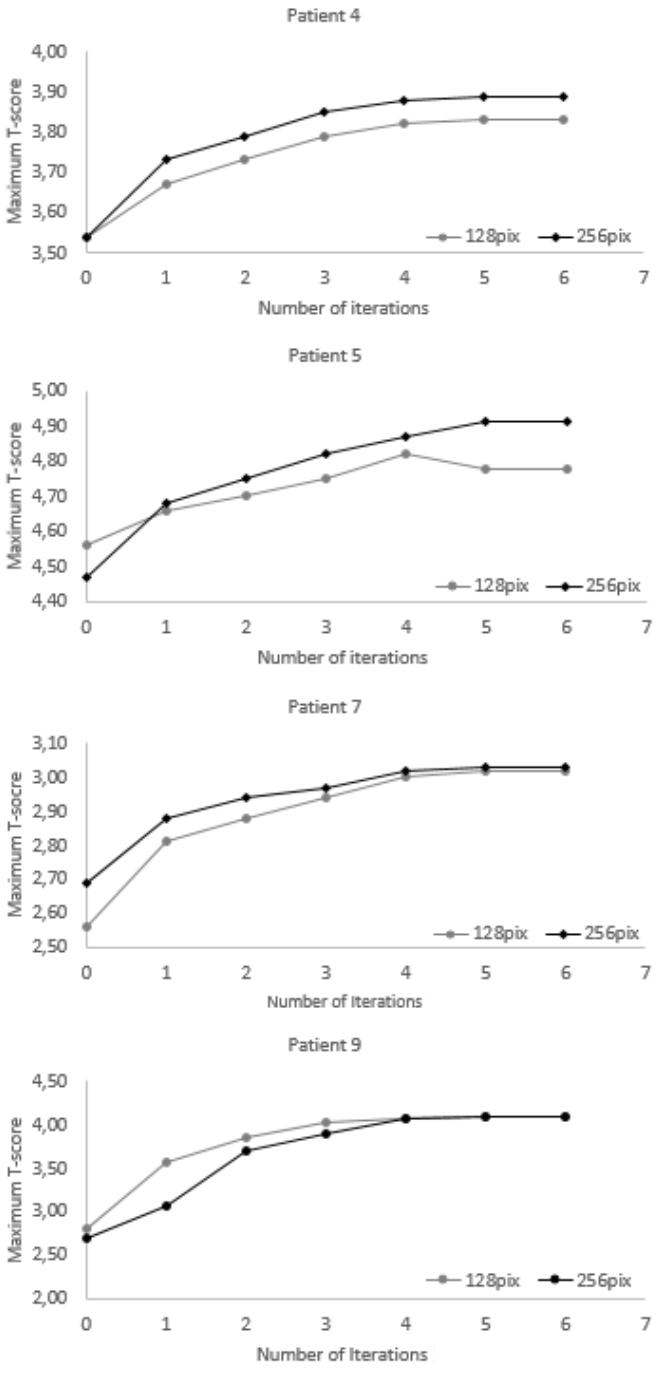

Figure 5: Variation of the SPM T-score values with the number of iterations for 4 of our patients. Patients 4 and 5 are examples of extended hypometabolisms, while patients 7 and 9 are examples of focal hypometabolisms.

localization for 14/18 patients (78%) for uncorrected images, 15/18 (83%) for SFS-RR corrected images and 17/18 (94%) for iSFS-RR. Table 2 shows the full PET reports obtained with uncorrected images, SFS-RR and iSFS-RR.

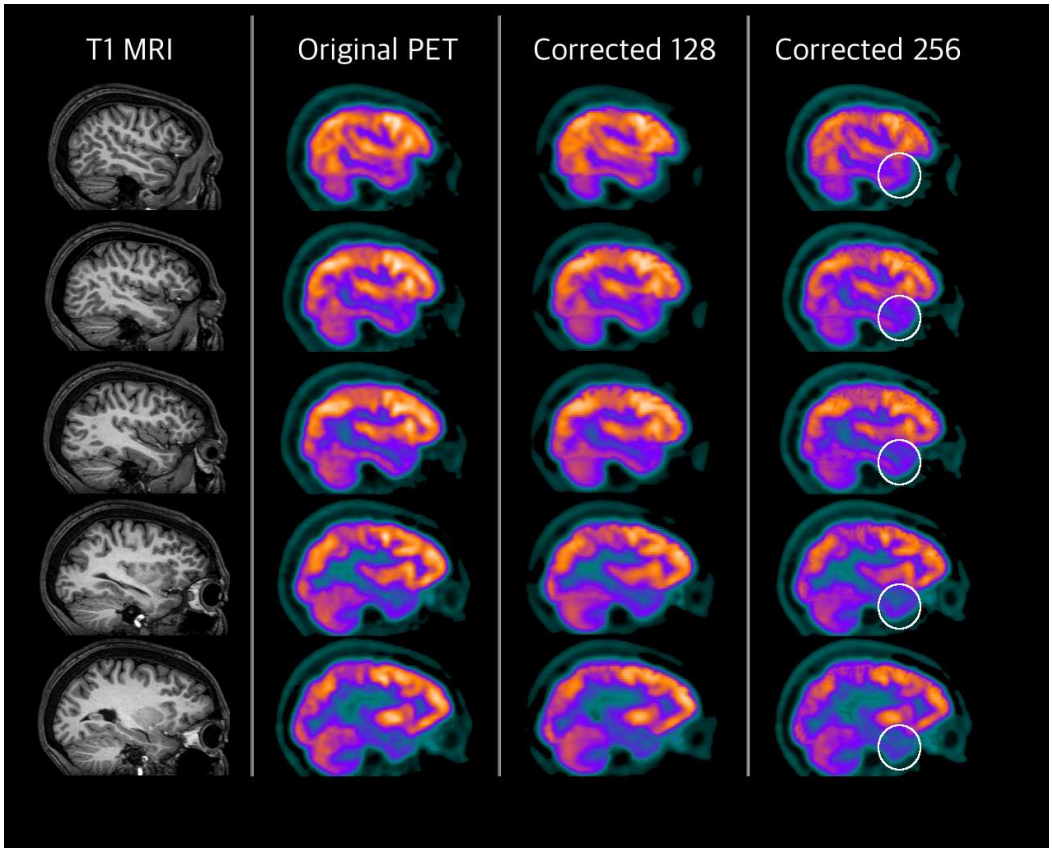

Figure 6: Visual comparison of original PET, 128 pixels and 256 pixels corrected images. On the image, coronal slices of the temporal lobe of a pathological patient. White circle points the lesion

IV. Discussion

The application of PET in neurological diseases related with small focal hypometabolic areas have been usually hindered by the limited resolution. Improving this can be performed using two main approaches: image reconstruction with PSF modeling, which can include the use of anatomical priors to guide the regularization, or by applying post-reconstruction PVE correction methods [14]. These last techniques are based on image enhancement by post-processing, either by deconvolution or by incorporating high frequency information taken from a structural image [31]. These techniques have particular advantages compared with the PSF modeling approach, mainly better noise handling. In Shidahara et al. (2009) [18], it was shown that improved performance of these wavelet-based methods could be achieved by using a segmented atlas image instead of the raw CT or MR data. An important limitation of this approach is that the PET is used to construct the segmented atlas, and this information, affected by PVE, can limit the effectiveness of the RR technique. This work aimed at the evaluation of an iterative application of the SFS-RR that can potentially solve this issue. The proposed methodology has points in common with the iterative Yang 1 proposed by Erlandsson et al [14], where instead of using the WT the authors propose an iterative correction based on the region-based voxel-wise correction (RVB). The methodology for updating the source image is similar to the 'iterative partial volume effect correction' (itPVEC) recently proposed by Shcherbinin and Celler [32]. An assessment of the proposed methodology was firstly carried out in terms of convergence and input image sizes. The study of convergence showed that iSFS-RR converges after 6 iterations, providing differences between consecutive images below 5% (maximum) and 2% (average). The performance of the proposed methodology in terms of input image sizes showed that AIs and T-score values were increased with respect to uncorrected images similarly for 128 and 256 input image sizes, after 6 iterations. In particular, the latter study showed that T-score values were significantly increased for the focal hypometabolisms, both for 128 and 256 input image sizes, thus showing that the good quantitative performance of the proposed iSFS-RR. We concluded that the quantitative improvement was similar regardless of the input image size, thus showing that time performance can be improved by a factor three without significant changes in iSFS-RR outcome.

	Visual Inspection PET/MR			Asymmetry Indexes			SPM Stat Analysis			Final PET Report		
N	Original	SFS-RR	I-SFS-RR	Original	SFS-RR	I-SFS-RR	Original	SFS-RR	I-SFS-RR	Original	SFS-RR	I-SFS-RR
1	-	-	1	6.4%	6.67%	6.9%	-	-	-	-	-	1
2	1	1	1	6.18%	6.44%	6.63%	-	-	3.72	1	1	1
3	1	1	1	7.57%	7.4%	7.52%	-	3.56	3.75	1	1	1
4	1	1	1	9.54%	9.48%	9.34%	6.34	6.44	6.50	1	1	1
5	1	1	1	8.76%	8.89%	8.93%	4.28	4.42	4.71	1	1	1
6	1	1	1	10.34%	10.21%	10.11%	5.44	5.49	5.53	1	1	1
7	1	1	1	7.20%	7.20%	7.19%	-	3.65	4.10	1	1	1
8	-	1	1	-	-	-	-	3.67	3.87	-	1	1
9	1	1	1	9.1%	9.75%	10.18%	4.47	4.81	4.91	1	1	1
10	-	-	1	-	-	7.5%	-	-	-	-	-	1
11	1	1	1	8.97%	9.52%	10.45%	3.86	4.87	5.56	1	1	1
12	1	1	1	9.45%	9.67%	10.18%	3.56	3.67	3.88	1	1	1
13	1	1	1	12.57%	12.52%	12.42%	4.14	4.32	4.49	1	1	1
14	1	1	1	6.07%	6.01%	6.09%	-	-	-	1	1	1
15	1	1	1	8.27%	9.05%	9.21%	-	-	3.54	1	1	1
16	1	1	1	8.81%	8.52%	8.21%	3.54	3.84	3.89	1	1	1
17	-	-	-	5.51%	5.21%	-	-	-	-	-	-	-
18	1	1	1	13.82%	13.42%	13.31%	4.67	4.98	5.11	1	1	1

Table 2: Results of the visual inspection, the AIs quantification and the SPM stat analysis for our group of 18 patients and for uncorrected images, SFS-RR corrected images and for iSFS-RR corrected images. On this table, 1 represents a true positive while "-" represents a negative. The SPM columns reflect the maximum values within the clusters.

After validation and optimization of the methodology, the technique was applied to a group of 18 patients previously diagnosed with refractory epilepsy. Comparisons in terms of sensitivity between uncorrected images, SFS-RR and iSFS-RR images were carried out. Regarding the visual inspection, sensitivity was improved from 78% to 83% and 94% with SFS-RR and iSFS-RR respectively. It has to be mentioned that the physicians also gave overall a more complete description of the lesions for iSFS-RR and SFS-RR, especially when the hippocampus was involved. Regarding the quantitative evaluation, the sensitivity of SPM scores was increased from 50% for uncorrected images to 66% for SFS-RR images and 83% for iSFS-RR images. This is due to that corrected images have better contrast and therefore T-scores values are increased so that more significant differences between the patient and the control group can be reported. The sensitivity of AIs evaluation was 88% regardless of used image, thus showing that the spatial resolution improvement derived from SFS-RR and iSFS-RR corrections does not affect AIs values. This can be explained by the size of the involved ROIs, where the exchanges of counts will happen mainly between white and grey matter within the ROI. Regarding the final report, the sensitivity of the combined evaluation was increased from 78% to 83% for SFS-RR and 94% for iSFS-RR. Although this was mainly derived from the better localization on the visual inspection, it is valuable to mention that iSFS-RR improved the SPM sensitivity, leading to better sensitivities both on visual and SPM evaluations. This is a valuable result for increasing the contribution of quantification to the process.

V. Conclusions

A method for the improvement of brain PET spatial resolution based on MRI information was developed and clinically evaluated in patients with epilepsy. Our findings showed that iSFS-RR provided an improved localization of small focal hypometabolisms and consequently an increase in the sensitivity of the diagnosis from 78% to 94%. Furthermore, iSFS-RR improved the sensitivity of the SPM analysis, which is essential for its future integration in clinical routine.

VI. Acknowledgements

The authors would like to thank Dr. Miho Shidahara and Prof. Alexander Hammers for their valuable advice and for providing the tools that made this work possible. In addition, to all the colleagues in the Division of Biomedical Imaging of the University of Leeds for their support and their hospitality.

VII. Bibliography

[1] YF. Tai and P. Piccini, "Applications of positron emission tomography (PET) in neurology," *J Neurol Neurosurg Psychiatry*, no. 75, pp. 669-676, 2004.

[2] M. Politis and P. Piccini, "Positron emission tomography imaging in neurological disorders.," *J Neurol*, vol. 259, no. 9, pp. 1769-80, 2012.

[3] BM Fuster et al., "FocusDET, a new toolbox for SISCOM analysis. Evaluation of the registration accuracy using Monte Carlo simulation," *Neuroinformatics*, vol. 11, no. 1, pp. 77-89, 2013.

[4] SS. Spencer, "The relative contributions of MRI, SPECT, and PET imaging in epilepsy.," *Epilepsia*, vol. 35, no. Suppl 6, pp. 72-89, 1994.

[5] HJ. Won et al., "Comparison of MR Imaging with PET and IctalSPECT in 118 Patients with Intractable Epilepsy," *AJNR*, vol. 20, pp. 593-599, 1999.

[6] H. Kassem et al., "Presurgical evaluation of refractory temporal lobe epilepsy: Comparison of MR imaging, PET and ictal SPECT in localization of the epileptogenic substrate," *EJRNM*, vol. 44, no. 3, pp. 641–649, 2013.

[8] YK. Kim et al., "(18)F-FDG PET in localization of frontal lobe epilepsy: comparison of visual and SPM analysis," *J Nucl Med*, vol. 43, no. 9, pp. 1167-74, 2002.

[7] HW. Shin et al., "Hybrid PET/MR May Improve Diagnostic Yield of Epileptic Lesions," *Neurology*, vol. 84, no. 14, p. P6, 2015.

[9] SK Lee et al., "FDG-PET Images Quantified by Probabilistic Atlas of Brain and Surgical Prognosis of Temporal Lobe Epilepsy," *Epilepsia*, vol. 43, no. 9, pp. 1032-1038, 2002.

[10] A Desai et al., "Interictal PET and ictal subtraction SPECT: sensitivity in the detection of seizure foci in patients with medically intractable epilepsy.," *Epilepsia*, vol. 54, no. 2, pp. 341-50, 2013.

[11] CH. Wong et al., "Relationship between preoperative hypometabolism and surgical outcome in neocortical epilepsy surgery," *Epilepsia*, vol. 53, no. 8, pp. 1333-1340, 2012.

[12] OG Rousset, DL Collins, A Rahmim, and DF Wong, "Design and implementation of an automated partial volume correction in PET: application to dopamine receptor quantification in the normal human striatum ," *J Nucl Med*, vol. 49, pp. 1097-1106, 2008.

[13] D Strul and B Bendriem, "Robustness of anatomically guided pixel-by-pixel algorithms for partial volume effect," *J Cereb Blood Flow Metab*, vol. 19, pp. 549-57, 1999.

[14] K. Erlandsson, I. Buvat, PH. Pretorius, BA. Thomas, and BF. Hutton, "A review of partial volume correction techniques for emission tomography and their applications in neurology, cardiology and oncology.," *Phys Med Biol*, vol. 57, no. 21, pp. 119-59, 2012.

[15] A Rahmim, J Qi, and V Sossi, "Resolution modeling in PET imaging: Theory, practice, benefits, and pitfalls," *Med Phys*, vol. 40, no. 6, 2013.

[16] B Bai, Q Li, and RM Leahy, "MR Guided PET Image Reconstruction," *Semin Nucl Med*, vol. 43, no. 1, pp. 30-44, 2013.

[18] M. Shidahara et al., "Functional and structural synergy for resolution recovery and partial volume correction in brain PET ," *Neuroimage*, vol. 44, no. 2, pp. 340-8, 2009.

[17] MJ Ehrhardt et al., "Joint reconstruction of PET-MRI by exploiting structural similarity," *Inverse Problems*, vol. 31, no. 1, 2014.

[19] N del Campo et al., "Quantification of receptor-ligand binding potential in sub-striatal domains using probabilistic and template regions of interest," *Neuroimage*, vol. 55, no. 1, pp. 101-12, 2011.

[20] CJ. McGinnity et al., "Quantification of opioid receptor availability following spontaneous epileptic seizures: correction of [11C]diprenorphine PET data for the partial-volume effect.," *Neuroimage*, vol. 79, pp. 72-80, 2013.

[21] E. Kim et al., "Partial volume correction using structural-functional synergistic resolution recovery: comparison with geometric transfer

matrix method.," *J Cereb Blood Flow Metab*, vol. 33, no. 6, pp. 914-20, 2013.

[22] M. Shidahara et al., "Wavelet-based resolution recovery using an anatomical prior provides quantitative recovery for human population phantom PET [^{11}C]raclopride data.," *Phys Med Biol*, vol. 57, no. 10, pp. 3107-22, 2012.

[23] E Grecchi et al., "Multimodal Partial Volume Correction – Application to [18F]Fluoride PET/CT bone metastases studies," *J Nucl Med*, vol. In Press, 2015.

[24] J Nunez, X Otazu, and MT Merino, "A multiresolution-based method for the determination of the relative resolution between images: first application to remote sensing and medical images. ," *Int. J. Imaging Sys. Tech.* , vol. 15, pp. 235-255, 2005.

[25] N Boussion et al., "A multiresolution image based approach for correction of partial volume effects in emission tomography.," *Phys Med Biol*, vol. 51, no. 7, pp. 1857-76, 2006.

[26] I Selesnick and KL Li, "Video denoising using 2D and 3D dual-tree complex wavelet transforms: Wavelet applications in signal and image processing. ," *Proc. of SPIE* , pp. 607-661, 2003.

[28] A. Hammers et al., "Three-dimensional maximum probability atlas of the human brain, with particular reference to the temporal lobe," *Hum Brain Mapp*, vol. 19, no. 4, pp. 224-47, Aug 2003.

[27] A Collignon et al., "Automated multi-modality image registration based on information theory," *Bizais*, 1995.

[29] J Ashburner and KJ Friston, "Unified segmentation," *NeuroImage*, vol. 26, pp. 839–851, 2005.

[30] D Perani et al., "Validation of an optimized SPM procedure for FDG-PET in dementia diagnosis in a clinical setting," *Neuroimage Clin*, vol. 6, pp. 445-54, 2014.

[31] A Le Pogam et al., "Evaluation of a 3D local multiresolution algorithm for the correction of partial volume effects in positron emission tomography.," *Med Phys*, vol. 38, no. 9, pp. 4920-23, 2011.

[32] S Shcherbinin and A Celler, "Assessment of the severity of partial volume effects and the performance of two template-based correction methods in a SPECT/CT phantom experiment," *Phys Med Biol*, vol. 56, no. 16, pp. 5355-71, 2011.

[33] K Erlandsson and B Hutton, "A novel voxel-based partial volume correction method for single regions of interest," *J Nucl Med*, vol. 55, no. Suppl 1, p. 2123, 2014.